Int. J. Electrochem. Sci., 15 **(2020)** 10955 – 10970, doi: 10.20964/2020.11.72

International Journal of
ELECTROCHEMICAL
SCIENCE
www.electrochemsci.org

Effect of Selected Process Parameters on Efficiency Enhancement of Electrochemical Etching and Polishing of Tungsten under Forced Convection

Yuanlong Chen[*]*, Peixuan Chen, Hua Lin, Xiang Li*

School of Mechanical Engineering, Hefei University of Technology, Hefei 230009, China
[*]E-mail: chenyuanlong@mail.hfut.edu.cn

Received: 23 July 2020 / *Accepted:* 11 September 2020 / *Published:* 30 September 2020

Tungsten coating of the thermionic emitter of the thermionic energy converter (TEC) was electrochemical polished (ECP) and etched (ECE) to enhance the electronic work function of the coating. The machining efficiency of these two electrochemical processes can be improved by using forced convection in alkaline solution. The tungsten anodic dissolution under forced convection in NaOH solution can be divided into the etching stage and the polishing stage according to the relationship between the current density and the applied voltage and the surface morphology. The influences of electrode distance, flow rate and NaOH concentration on the current density of tungsten anodic dissolution were analyzed. The current density can be enhanced by selecting these process parameters rationally and the efficiency of ECE or ECP is improved.

Keywords: Tungsten; Forced convection; Electrochemical etching; Electrochemical polishing; Current density

1. INTRODUCTION

Due to the high power density, long power output duration, and no need to harvest solar energy, thermionic energy converter (TEC) is widely utilized in spacecrafts, especially for deep space exploration. Thermionic emitter, which operates at a high ambient temperature, is an important component of TEC. Tungsten is the most suitable material for the coating of thermionic emitter due to its excellent properties, including a high melting point, low saturated vapor pressure, high temperature creep resistance, and high work function of thermionic emission [1-3]. The electronic work functions of crystal planes of tungsten crystal have anisotropic characteristics, which are arranged in the following decreasing order: {110}> {112}> {100}> {111} [4]. Since the {110} plane has the highest electronic work function, it is more suitable for the surface of thermionic emitter than other crystal planes of

tungsten. Owing to the anisotropy of anodic dissolution of tungsten crystal planes in the same electrolyte and a strong preferential attack on the weak atomic planes except {110} plane, {110} plane can be exposed to a higher degree on the surface of thermionic emitter through electrochemical etching (ECE), which increases the proportion of {110} plane on the emitter coating. For eliminating the surface impurity, residual scratches of mechanical polishing, and subsurface damage layer of the emitter coating, electrochemical polishing (ECP) has been indispensably performed on the tungsten coating before ECE of the thermionic emitter [5, 6].

As early as 1959, Hughes et al. [7] prepared a wire with a coating of tungsten single crystal using a thermal gradient technique and etched its surface in a room temperature solution of 70% HNO_3:30% HF. They found that {110} and {112} planes were left on the wire surface after etching for 2 min. Thompson et al. [5] pointed out that there is a strong preferential attack on the weak atomic planes during ECE of tungsten, thereby leaving a flat surface of {110} plane with high surface density. In 2016, Mu et al. [6] conducted experiments on ECE of tungsten monocrystal and polycrystal. Further, they proposed a method for determining the proportion of {110} planes on the tungsten surface of monocrystal coating, which was based on direct observation using an autofocusing microscope. Wang et al. [8] provided a comprehensive study on the anodic behavior of tungsten during ECP and suggested that ECP of tungsten could be divided into 3 stages including the etching stage in which crystallographic etching occurred, the brightening stage in which ultra-smooth surfaces were obtained, and the pitting stage in which crystallographic pitting occurred. However, the above studies primarily focused on ECE or ECP of tungsten under natural convection. The anodic dissolution of tungsten under forced convection and the effects of processing parameters on ECE and ECP of tungsten have been rarely reported.

Over the past few decades, several researches have investigated the electrochemical behavior of tungsten and the formation of anodic oxide films on tungsten in various electrolyte solutions with pH 0 to 14 [9-16]. The main conclusion of these studies is that the anodic dissolution behavior of tungsten depends on the pH of electrolyte, i.e., the ion concentration of H^+ and OH^- in electrolyte impacts the anodic oxidation of tungsten. Additionally, oxide films on tungsten surface have been confirmed to play a prominent role in the anodic dissolution of tungsten. The WO_3 film formed on the surface, which is generated during the anodic oxidation of tungsten, is slightly soluble in acidic or neutral solutions [14, 17, 18], but it can be completely dissolved in alkaline solutions. The anodic dissolution rate of tungsten in acidic or neutral solutions is much lower than that in alkaline solutions due to the inhibition of WO_3 film [11, 19]. Hence, high electrochemical processing efficiency of tungsten can be acquired by using alkaline solutions. Since the limiting current density for the anodic dissolution of tungsten is determined by the mass transfer of OH^- ion when the pH is above 12.5 [9], the effects of processing parameters that affect the diffusion of OH^- ion should be examined while studying the electrochemical processing of tungsten.

In this study, the anodic dissolution of tungsten was conducted under forced convection in NaOH solution. The influence of some critical electrochemical processing parameters such as electrode distance, flow rate, and NaOH concentration on the efficiency of ECE and ECP of tungsten were experimentally analyzed. Overall, this study can serve as a useful reference for selecting process parameters of ECE and ECP under forced convection to optimize the electrochemical processing efficiency of tungsten.

2. EXPERIMENTAL

The investigated materials were cut from a tungsten rod (99.95% purity) using wire electrical discharge machining and were machined into specimens with the diameter of 8 mm and length of 8 mm. An electrode of stainless steel (AISI 304) was used as the cathode. A self-designed experimental setup is shown schematically in Figure 1. The flow channel was constituted by the upper chamber and the lower chamber, which were manufactured from glass fibre reinforced plastics (GFRP). The electrolyte was pumped from the electrolyte tank into the flow channel by a centrifugal pump. The adjustment of the pressure and velocity of the electrolyte flow was realized by a three-way valve.

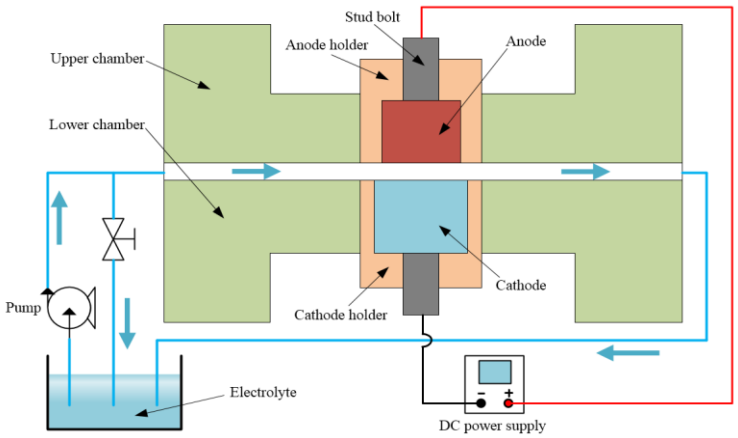

Figure 1. Schematic of experimental setup

Tungsten anodic dissolution which based on the simultaneous anodic oxidation takes place on the anode surface and the anodic oxidation is an electrochemical multistep reaction in alkaline solutions. Firstly, tungsten is oxidized to WO_2 and WO_2 forms oxide films on the anode surface. Afterwards WO_2 is oxidized into WO_3. There is a chemical reaction that WO_3 can react with NaOH solution and thus dissolves into the electrolyte. The oxidation reaction on the anode and the following reaction in NaOH solution are expressed as follows [9,12,19]:

Anode: $W(s) + 4OH^- \rightarrow WO_2(s) + 2H_2O + 4e^-$ (1)

$WO_2(s) + 2OH^- \rightarrow WO_3(s) + H_2O + 2e^-$ (RDS) (2)

Following reaction: $WO_3(s) + 2OH^- \rightarrow WO_4^{2-} + H_2O$ (3)

The overall anodic reaction can be written as

$W + 8OH^- \rightarrow WO_4^{2-} + 4H_2O + 6e^-$ (4)

The reduction reaction occurs on the stainless-steel cathode is the electrolysis of water and generates hydrogen gas, it can be expressed as Equation (5):

Cathode: $6H_2O + 6e^- \rightarrow 3H_2(g) + 6OH^-$ (5)

The limiting anodic current of tungsten dissolution is totally controlled by OH^- ion diffusion to the anode surface when pH is above 12.5. Equation (2) is the rate-determining step (RDS) of tungsten anodic oxidation. Considering that forced convection can promote the diffusion of OH^- ion, various

concentration solutions of NaOH and fluid flow of various velocities were used in this study. The process parameters used in the study of tungsten anodic dissolution is listed in Table 1. In order to investigate the anodic dissolution behavior of tungsten, the relationships between the current density and the applied voltage under different process parameters were obtained by potentiostatic method.

Table 1. The process parameters of tungsten anodic dissolution

Parameter	Value	Unit
Applied voltage	1.3 to 30	V
Electrolyte flow rate	1.3, 2.0, 3.3	m/s
NaOH concentration	0.7, 1.0, 1.5	wt%
Electrode distance	1, 2, 3	mm
Electrolyte temperature	20	^{0}C

Before and after every experiment, the specimens were rinsed with alcohol and dried by compressed air. A surface roughness tester (TIMEZY TR210) was utilized to measure the studied surfaces. The specimen surface morphology was characterized by a scanning electron microscopy (SEM, Hitachi SU8010).

3. RESULTS AND DISCUSSION

3.1. Etching stage and polishing stage

The variation in anodic current as a function of applied voltage was measured under the electrode distance of 3 mm and flow rate of 1.3 m/s in 1 wt% NaOH solution. The results are shown in Figure 2. It is clear that the anodic current density rapidly increases with the applied voltage when the applied voltage is below 4.5 V (green vertical line). As the applied voltage further increases in the range of 4.5 V to 30 V, the anodic current density tends to become flat and increases slowly from 0.45 A/cm^2 to 0.56 A/cm^2. Initially, the current density rises sharply with the increasing in the applied voltage, which indicates that the anodic dissolution of tungsten is controlled by electrochemical polarization when a lower voltage is applied. While the applied voltage is higher than a 'valve value', e.g., 4.5 V under the above electrochemical processing conditions, the current density exhibits a minor increase. It can be concluded that when the applied voltage is above the 'valve value', the anodic dissolution of tungsten is determined by the limiting current density, which is mainly controlled by the mass transfer of OH^- according to Equation (2) [19, 20]. Therefore, the anodic dissolution of tungsten can be divided into two stages: one stage is controlled by the electrochemical polarization and the other is controlled by the diffusion of OH^- ion.

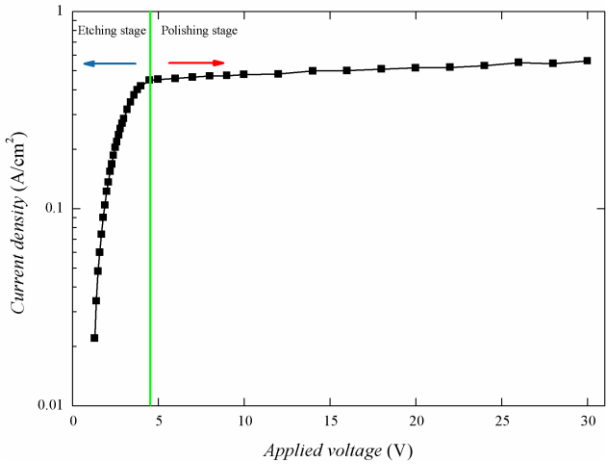

Figure 2. Relationship between current density and applied voltage under NaOH concentration of 1 wt%, electrode distance of 3 mm, and flow rate of 1.3 m/s

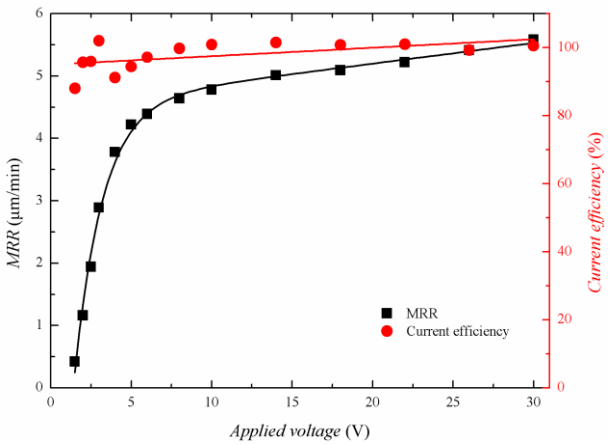

Figure 3. Variation in MRR and current efficiency as a function of applied voltage under NaOH concentration of 1 wt%, electrode distance of 3 mm, and flow rate of 1.3 m/s

For analyzing the impact of electrochemical polarization and the diffusion of OH^- on the tungsten anodic dissolution, we implemented experiments to measure the material remove rate (MRR), the current efficiency, and the surface roughness and to characterize the morphology of tungsten surface after anodic dissolution.

MRR was calculated by the following Equation (6):

$$v_a = \frac{m_0 - m}{\rho A t} \qquad (6)$$

where v_a represents MRR, m_0 is the initial mass of specimen, m is the specimen mass after experiment, ρ is the density of tungsten, A is the anode surface area, and t is the processing duration.

The current efficiency can be expressed as follows:

$$\eta = \frac{m_0 - m}{\omega It} \times 100\% \quad (7)$$

where η represents the current efficiency, ω is the mass electrochemical equivalent of hexavalent tungsten, I indicates the anodic current, and m_0, m, and t are explained in Equation (6).

Figure 3 shows the variation in MRR and the current efficiency as a function of applied voltage were under the following processing conditions: electrode distance = 3 mm, flow rate = 1.3 m/s, NaOH concentration = 1 wt%, and duration = 5 min. It is evident that the MRR rises steeply with the increase in applied voltage when the voltage is lower than 5 V. When the voltage is higher than 5 V, MRR tends to be stable and increases slightly with the increase in applied voltage. The measured current efficiency under different voltages ranges from 88% to 102%. The current efficiency for the anodic dissolution of tungsten in NaOH solution is close to 100%. Based on the results in Figure 2, which are obtained under the same condition, the variation trend of MRR is basically consistent with that of current density. Therefore, MRR is proportional to the current density and can be improved by increasing the current density.

The measured values of mean roughness (Ra) of tungsten surface after anodic dissolution are shown in Figure 4. It is clear that the value of Ra decreases with the increase in the applied voltage when the voltage is below 5 V. When the voltage is above 5 V, the value of Ra continues to decrease and finally reaches 0.137 μm.

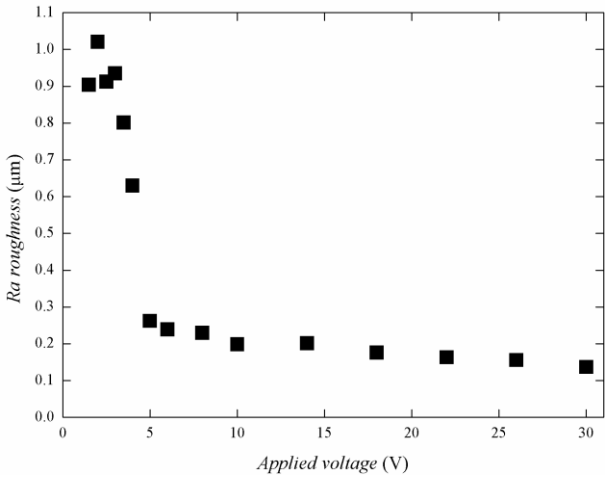

Figure 4. Variation in the value of Ra as a function of applied voltage under NaOH concentration of 1 wt%, electrode distance of 3 mm, and flow rate of 1.3 m/s

The images of two tungsten specimens after anodic dissolution under electrode distance of 3 mm, flow rate of 1.3 m/s, and NaOH concentration of 1 wt% are shown in Figure 5. The specimen shown in Figure 5(a) was obtained under an applied voltage of 4 V and processing duration of 1 min, where 4 V is close to the 'valve value'. The blue arrow in Figure 5(a) indicates the direction in which the electrolyte flows through the specimen surface. It is obvious that the specimen surface can be divided into three areas along the flow direction. The surface of area I near the electrolyte inlet is rough and no mirror

effect can be observed. The surface of area III near the electrolyte outlet is relatively smooth, and the polishing effect is obviously better than that of area I. The transition area II between areas I and III is a matte-like surface, which is smoother than area I and rougher than area III. Figure 5(b) shows another specimen, which is processed under 30 V for 5 min. It is clear that the entire processed surface is completely polished and bright. Wang et al. obtained the polishing effect by using a higher concentration of NaOH under natural convection for 10 min [8], while ECP based on forced convection take less time and is more efficient than ECP under natural convection.

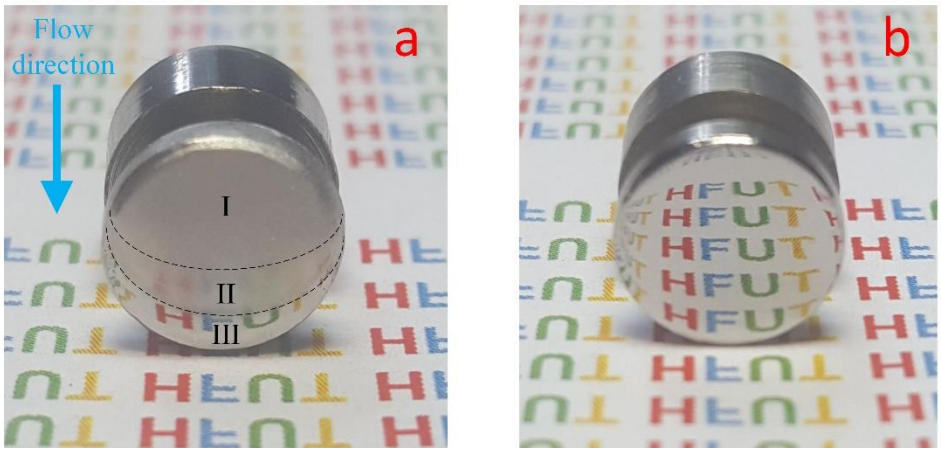

Figure 5. Photos of tungsten specimens after anodic dissolution under the conditions of (a) applied voltage: 4 V, NaOH concentration: 1 wt%, electrode distance: 3 mm, processing duration: 1 min, (b) applied voltage: 30 V, NaOH concentration: 1 wt%, electrode distance: 3 mm, processing duration: 5 min

The typical surface morphologies of the two tungsten specimens were examined by SEM. The SEM images of area I, II, and III in Figure 5(a) are shown in Figure 6(a), (b), and (c), respectively. It is clear from Figure 6(a) that the surface of area I is seriously etched and shows very rough. Based on the Hoar's passivation theory [21], the polishing effect can be achieved due to the inhibition of etching by the passivation film formed between the anode and the electrolyte during ECP. It can be concluded that sufficient OH^- ions react with WO_3 so that the WO_3 film on the surface can rapidly dissolve into electrolyte, and there is no WO_3 film covering the surface of area I. In Figure 6(b), the surface of area II is also etched, but it is not as rough as that of area I. The obvious crystallographic etching leads to the formation of many step-like etching marks on the surface of area II, which can be explained by the terrace-ledge-kink (TLK) model [22]. Due to the preferential etching along the particular orientations, the dissolution rate of less-packed crystal plane is higher than of close-packed crystal plane, so grains on the surface tend to expose terraces composed of close-packed crystal planes. Figure 6(c) shows that grain boundaries are strongly corroded.

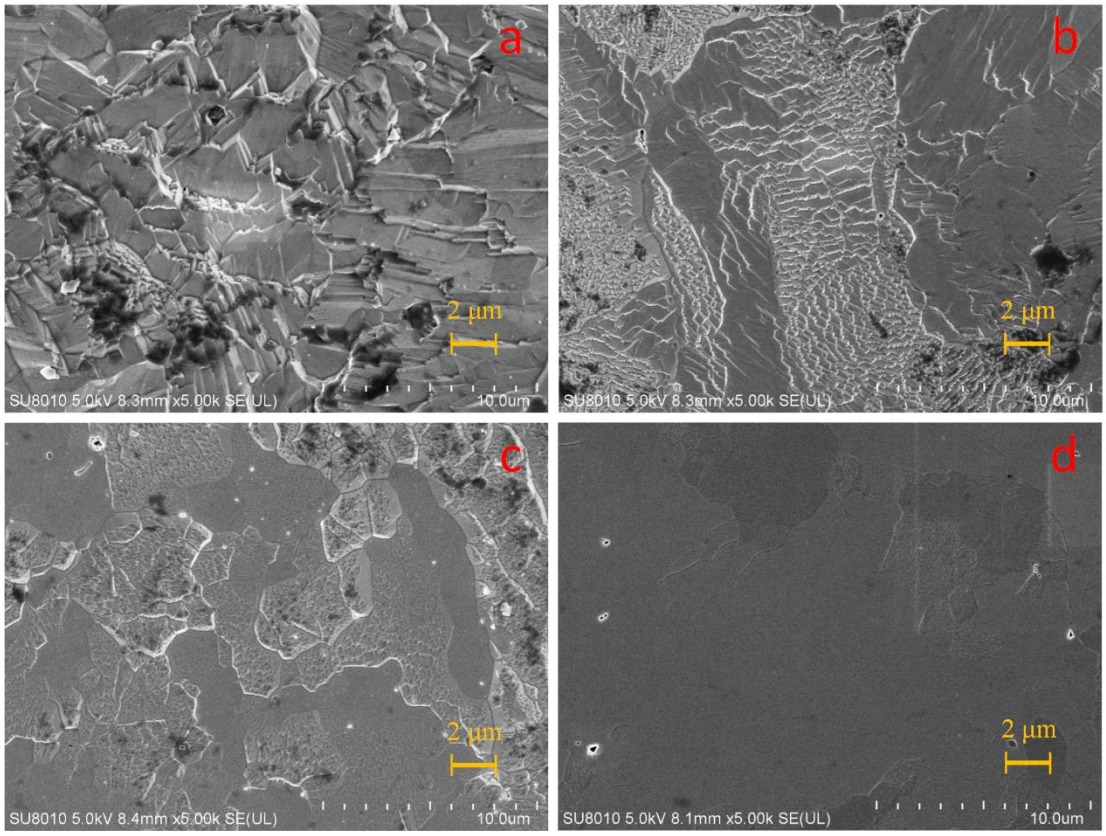

Figure 6. SEM images of tungsten surfaces of (a) area I in Figure 5(a), (b) area II in Figure 5(a), (c) area III in Figure 5(a), (d)Figure 5(b)

Further, some grains are slightly etched, while some grains are free of etching marks. Thus, the surface of area III is smoother than that of area II, which can also be seen from Figure 5(a). Along the flow direction, most of the OH^- ions are consumed on the surface of area I that is near the flow inlet, resulting in an insufficient concentration of OH^- ions on the surface of area that is far from the flow inlet. Consequently, the anodic dissolution on the surface of area II is controlled by both electrochemical polarization and the diffusion of OH^-, and a stable and permanent WO_3 film cannot be formed on the surface. Therefore, although crystallographic etching occurs on the surface of area II, it is not as rough as the surface of area I. After the OH^- ions are further consumed on area II, the anodic dissolution on area III is mainly controlled by the diffusion due to the lower OH^- concentration. Nevertheless, WO_3 film is not thick enough to completely prevent crystallographic etching of the entire surface of area III. The SEM image of specimen surface in Figure 5(b) is shown in Figure 6(d). It is clear that the surface is polished, and slight corrosion of grain boundary occurs on the surface. The specimen surface, which is processed under an applied voltage of 30 V, is much smoother than the surface of area III that is processed under 4 V. The anodic dissolution under 30 V is completely limited by the diffusion of OH^-, thus WO_3 film is thick enough to inhibit crystallographic etching.

According to the above experimental results and the relationship between current density and applied voltage, the stages in which the anodic dissolution of tungsten is controlled by electrochemical polarization and diffusion of OH^- can be defined as the etching stage and the polishing stage, respectively (see Figure 2).

3.2. Influence of flow rate

To investigate the impact of the flow rate on the electrochemical processing of tungsten, the dependence of the current density on the applied voltage was investigated under electrode distance of 3 mm in 1 wt% NaOH solution with flow velocities of 1.3, 2.0 and 3.3 m/s. The results are shown in Figure 7.

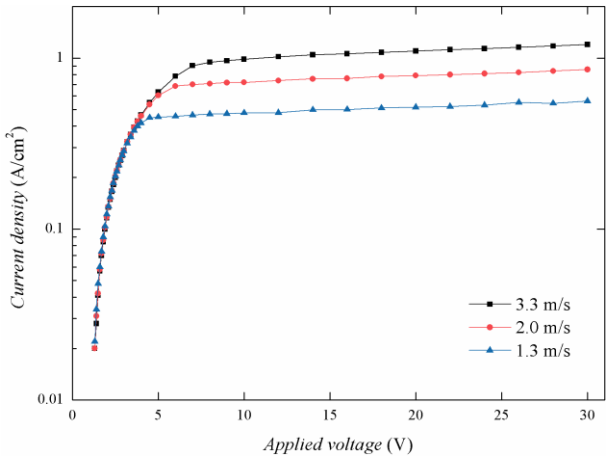

Figure 7. Relationship between current density and applied voltage under different flow rates ,where the electrode distance is 3 mm and NaOH concentration is 1 wt%

It is evident in Figure 7 that the current density approximately linearly proportional to the applied voltage under low voltage and grows slowly until it reaches the limiting current density in the etching stage. In the polishing stage, the current density reaches the plateau stage and increases slightly. The curves corresponding to different flow rates coincide with each other in the etching stage. It is noteworthy that the current densities of etching at different flow rates under the same voltage are almost identical, where the current densities under 1.7 V are 0.074, 0.072 and 0.070 A/cm^2 at flow rates of 1.3, 2.0 and 3.3 m/s, respectively. The difference is that the higher the flow velocity is, the wider the range of etching voltage. Additionally, the current density of polishing can be obtained at a higher flow rate, where the current density is 1.2 A/cm^2 at flow rate of 3.3 m/s and applied voltage of 30 V. Deng et al. [23] performed ECP under natural convection in 1 wt% NaOH solution with potential of 60 V, and the current density was only 0.2 A/cm^2. Obviously, the current density of ECP under forced convection is much higher than that under natural convection, indicating that ECP under forced convection is more efficient. Based on the relationship between current density and applied voltage under different flow rates, it may be conclude that the range of etching voltage and the current density of polishing are significantly affected by the flow rate.

According to the electrochemical polarization theory, the anodic current density only depends on the anodic overpotential, which is limited by the voltage between the electrodes and the resistance of the electrolyte. As the applied potential increases, the increased current density can lead to a higher consumption rate of reactants and a higher formation rate of reaction products. When the mass transfer

rate of reactants to the electrode surface or the rate at which reaction products leave from the electrode surface is lower than the electrochemical reaction rate, the mass transfer rate of reactants or reaction products is the RDS [24].

In this study, the current density of ECE for tungsten is controlled by electrochemical polarization. Irrespective of the value of flow rate, the resistance of the electrolyte between the electrodes cannot vary if the electrode distance is maintained and the heat and bubbles that are generated in the electrochemical processing can be immediately eliminated by electrolyte flow. Therefore, the experimental results show that the etching current densities are almost identical at different flow rates under the same voltage, and the curves coincide with each other well. The broadening of the range of etching voltage under forced convection can be attributed to the fact that the diffusion of OH^- is promoted by forced convection. According to Fick's law and convection-diffusion equation [25], the liquid flow can effectively reduce the thickness of the diffusion layer of OH^- ions, thereby enhancing the diffusion rate of OH^- [26]. When the diffusion rate of OH^- is sufficiently high, the current density is not controlled by RDS but is controlled by electrochemical polarization. A high flow rate can be used to enhance the etching voltage, thereby improving MRR of ECE for tungsten. Meanwhile, the machining efficiency of ECP for tungsten can be improved due to the increased current density in the polishing stage, which is obtained by using high flow rate.

3.3. Influence of NaOH concentration

The effect of the NaOH concentration must be considered because high concentration of electrolyte can promote the diffusion rate of OH^-. The dependence of current density on the applied voltage was examined under electrode distance of 3 mm and flow rate of 1.3 m/s with NaOH concentrations of 0.7, 1.0, and 1.5 wt%. The results are shown in Figure 8.

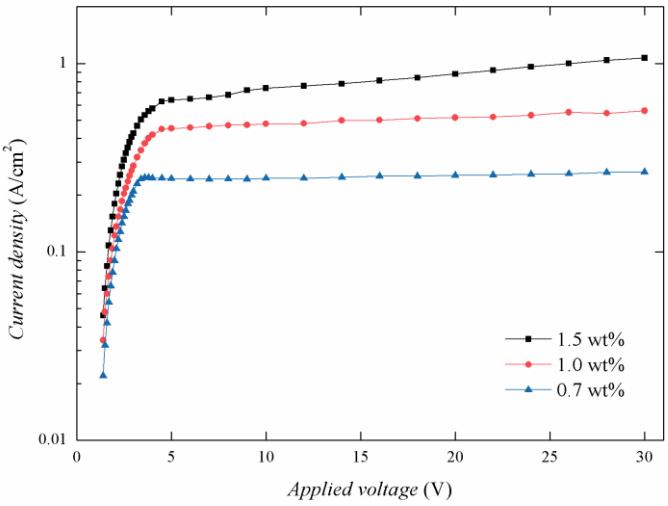

Figure 8. Relationship between current density and applied voltage under varying NaOH concentration, where the electrode distance is 3 mm and the flow rate is 1.3 m/s

The trend of the relationship between current density and applied voltage under forced convection in different NaOH solutions is basically the same as that under natural convection [19]. It is evident that the curves corresponding to different NaOH concentrations do not coincide completely with each other in the etching stage. When the applied voltage reaches a certain value, the current density tends to be stable, which indicates that the anodic dissolution of tungsten is in the polishing stage. As the NaOH concentration increases, the current density is improved in the etching stage. The current densities of etching under applied voltage of 2.3 V are 0.128, 0.168, and 0.256 A/cm^2 in 0.7, 1.0, and 1.5 wt% NaOH solutions, respectively. The limiting current density of tungsten polishing can reach up to 1.07 A/cm^2 in 1.5 wt% solution under 30 V, but the current density is limited to 0.266 A/cm^2 in 0.7 wt% solution. In addition, if a high concentration of electrolyte is used, the maximum value of etching voltage can be increased. The maximum etching voltage can reach 4.5 V in 1.5 wt% solution, whereas the maximum etching voltage can reach 3.4 V in 0.7 wt% solution. Overall, the effect of electrolyte concentration on the anodic dissolution of tungsten is that higher limiting current density can be achieved in the polishing stage by using higher concentration of electrolyte solution. Furthermore, under the condition of a high flow rate, the range of etching voltage can be extended by using a high concentration of electrolyte.

To explain the difference in the etching current densities under the same voltage at different flow rates, a simplified model is proposed and its schematic is shown in Figure 9. Several assumptions of the model are made as follows: (1) the electrical conductivity of electrolyte is independent of temperature and bubbles and thus is constant; (2) the electrical conductivities of both electrodes are much higher than that of electrolyte and the polarization overpotential of the electrode reaction is much lower than the voltage drop of the electrolyte, thus the applied voltage is equivalent to the voltage drop of the electrolyte [27, 28]. Therefore, the current density of tungsten anodic dissolution in the etching stage is determined by the resistance of electrolyte and by the applied voltage according to Ohm's law. The electrolyte resistance can be obtained as follows:

$$R_e = \frac{\Delta}{\kappa A} \quad (8)$$

where R_e is the electrolyte resistance, Δ is the electrode distance, κ is the electrical conductivity of electrolyte and A is the anode surface area.

The current density of tungsten anodic dissolution in the etching stage can be calculated by [29]:

$$j = \frac{U - Q}{R_e A} \quad (9)$$

where j represents the current density, U is the applied voltage, Q is the onset voltage of tungsten anodic dissolution in NaOH solution, R_e and A are expressed as Equation (8).

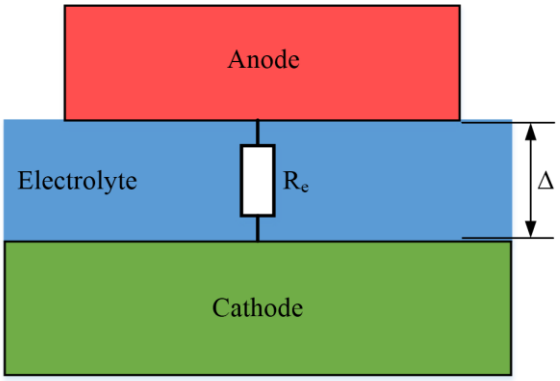

Figure 9. Schematic of the simplified model

In Figure 10, the current density values of ECE under applied voltage with various NaOH concentrations are shown as open dots. The relationship between current density and applied voltage were linearly fitted using least squares method, which are shown as dash lines. The onset voltages of different NaOH concentrations were obtained by extrapolating the linearly fitted lines (dash lines), which are 1.242, 1.212 and 1.238 V in 0.7, 1.0 and 1.5 wt% solution, respectively. Here the onset voltage was taken as 1.23 V. The relations of the current density depends on the applied voltage in different concentration solutions were calculated by using Equation (8) and (9) and the results are shown as full lines in Figure 10. It is obviously that the calculated results are basically consistent with the linearly fitted results of the experiments.

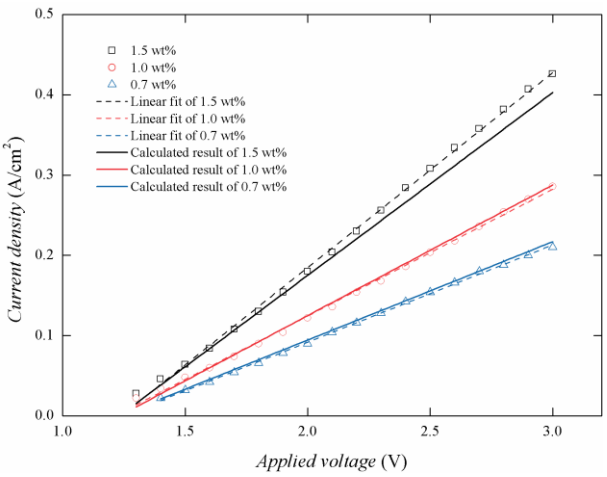

Figure 10. Curves of linear fit and calculated result with different NaOH concentrations in the etching stage

A higher conductivity of high concentration electrolyte leads to a lower resistance of the electrolyte, so higher etching current density can be achieved by using a high concentration solution. In addition, the electrical conductivity of electrolyte does not change with the flow rate. With the condition

of different flow rates and the same concentration solution, the current densities are nearly identical under the same voltage in the etching stage, as shown in Figure 7. It can be concluded that the etching current density is affected by the conductivity of electrolyte, which is mainly controlled by electrochemical polarization in the etching stage.

3.4. Influence of electrode distance

As the electrode distance plays a critical role in electrochemical processing, it is necessary to analyze the influence of electrode distance on the electrochemical processing of tungsten. Based on the above analysis, the anodic dissolution of tungsten is primarily determined by electrochemical polarization in the etching stage and diffusion rate of OH^- in the polishing stage. It can be deduced that the etching current density can be affected by the electrode distance, and smaller electrode distance can reduce the resistance of the electrolyte between both the electrodes. Thus, the etching current density is enhanced under a small electrode distance. The polishing current density, which is mainly controlled by the diffusion rate of OH^-, is strongly affected by the NaOH concentration and the flow rate, but it is weakly affected by the electrode distance. Since hydrogen bubbles generated by electrochemical processing under a small electrode distance can affect the conductivity of the electrolyte, higher flow rate is essentially adopted to eliminate the influence of bubbles [30]. To analyze the influence of electrode distance and verify the above viewpoint, the anodic dissolution of tungsten was experimentally investigated under electrode distance of 1, 2, and 3 mm with NaOH concentration of 1 wt% and flow rate of 2.0 m/s. The relationship between current density and applied voltage under different electrode distances is shown in Figure 11.

It is clear in Figure 11 that at the same applied voltage, higher current density is obtained by using a smaller electrode distance in the etching stage. Since it is difficult to guarantee the consistency of flow rate under different electrode distances, the values of polishing current density are slightly different, but the curves are approximately coincident with each other in the polishing stage. It can be concluded that the polishing current density is slightly affected by the electrode distance unless the electrode distance has a strong effect on the flow field distribution between the two electrodes, e.g., extremely small electrode distance and extremely high flow rate can lead to an uneven flow field distribution and flow cavitation. Based on the simplified model in section 3.3, the electrolyte resistances under different electrode distance were calculated by using Equation (9), and the results are shown as black squares in Figure 12. The electrolyte resistance R_e is linearly proportional to the electrode distance Δ according to Equation (8). The R_es vs. Δ curve is linearly fitted by least squares method, and which is shown as red line in Figure 12. Hence, the etching current density is significantly affected by the electrode distance.

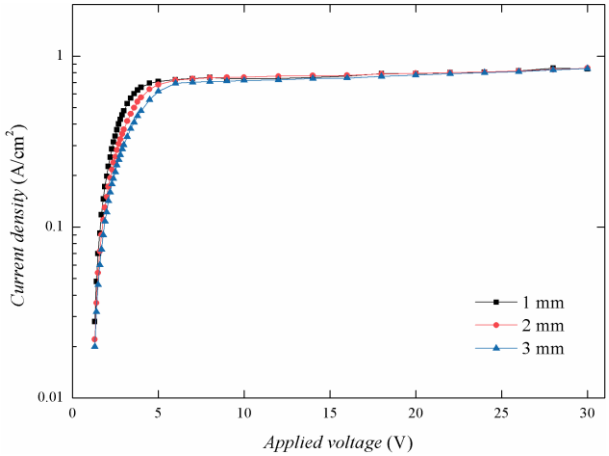

Figure 11. Relationship between current density and applied voltage under varying electrode distance, where the flow rate is 1.3 m/s and NaOH concentration is 1 wt%

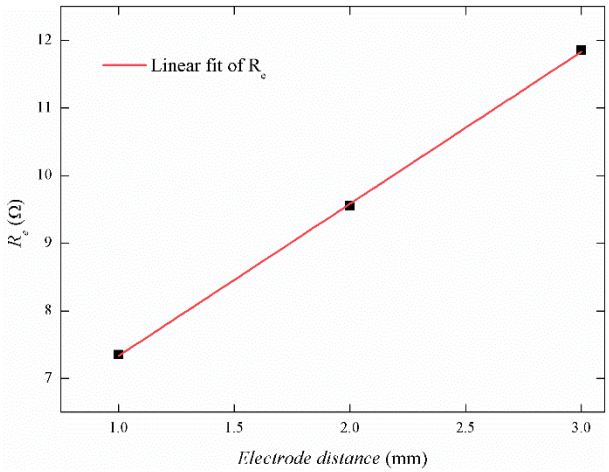

Figure 12. R_es calculated by the simplified model and the linear relation between R_e and the electrode distance

4. CONCLUSIONS

The anodic dissolution of tungsten was experimentally investigated under forced convection in NaOH solution. The electrochemical dissolution of tungsten was studied by examining the MRR, current efficiency, surface roughness, and surface morphology. Further, the effects of flow rate, NaOH concentration, and electrode distance on the efficiency of ECE and ECP of tungsten were analyzed. The main results of the study are summarized as follows:

(1) The anodic dissolution of tungsten under forced convection in NaOH solution could be divided into etching stage and polishing stage, where crystallographic etching occurred in the etching stage and a polished surface was obtained in the polishing stage. MRR was found to be proportional to the current density of anodic dissolution, and the efficiency of ECE and ECP could be improved by

increasing the current density.

(2) The voltage range of ECE under forced convection was widened under the condition of high flow rate and NaOH concentration. Thus, the current density of tungsten etching could be enhanced by using a high applied voltage. The tungsten etching, which was controlled by electrochemical polarization, was also affected by the electrode distance. A high etching current density could be obtained by using a small electrode distance under a uniform distribution of flow field.

(3) The effects of flow rate and NaOH concentration on the efficiency of ECP for tungsten were significant, which could be used to enhance the limiting current density. However, the electrode distance had a minor effect on the polishing current density. Consequently, to achieve a high polishing current density, the flow rate and NaOH concentration must be increased.

ACKNOWLEDGEMENTS
This work was financially supported by the National Natural Science Foundation of China (No. 51775161).

References

1. G.L. Bennett, R.J. Hemler, A. Schock, *J. Propuls. Power*, 12 (1996) 901.
2. J.Q. Shi, Y.B. Shen, S.Y. Yao, P.J. Zhang, Q. Zhou, Y.Z. Guo, C.W. Tan, X.D. Xu, Z.H. Nie, H.L. Ma, H.N. Cai, *Mater. Charact.*, 122 (2016) 36.
3. B-H Tsao, M.L. Ramalingam, B.D. Donovan, J.S. Cloyd, *AIP Conference Proceedings*, 217 (1991) 787.
4. R. Smoluchowski, *Phys. Rev.*, 60 (1941) 661.
5. J.R. Thompson, J.C. Danko, T.L. Gregory, H.F. Webster, *IEEE. T. Electron. Dev.*, 16 (1969) 707.
6. R.D. Mu, C.W. Tan, X.D. Yu, *J. Alloy. Compd.*, 666 (2016) 71.
7. F.L. Hughes, H. Levinstein, R. Kaplan, *Phys. Rev.*, 113 (1959) 1023.
8. F. Wang, X.Q. Zhang, H. Deng, *Appl. Surf. Sci*., 475 (2019) 587.
9. M. Anik, K. Osseo-Asare, *J. Electrochem. Soc.*, 149 (2002) B224.
10. T.H. Heumann, N. Stolica, *Electrochim. Acta.*, 16 (1971) 643.
11. J.W. Johnson, C.L. Wu, *J. Electrochem. Soc.*, 118 (1971) 1909.
12. G.S. Kelsey, *J. Electrochem. Soc.*, 124 (1977) 814.
13. M.S. El-Basiouny, M.M. Hefny, *Br. Corros. J.*, 16 (1981) 50.
14. V. Karastoyanov, M. Bojinv, *J. Solid. State.*, Electrochem. 13 (2009) 309.
15. T. Tuvić, I. Pašti, S. Mentus, *Russ. J. Phys. Chem. A+.*, 85 (2010) 2399.
16. A. Di Paola, F. Di Quarto, C. Sunseri, *Corros. Sci.*, 20 (1980) 1067.
17. M. Krebsz, J.P. Kollender, A.W. Hassel, *Phys. Status. Solidi. A.*, 214 (2017) 1600803.
18. A. Di Paola, F. Di Quarto, C. Sunseri, *Corros. Sci.*, 20 (1980) 1079.
19. T.H. Heumann, N. Stolica, *Electrochim. Acta.* 16 (1971) 1635.
20. M. Anik, T. Cansizoğlu, S. Çevik, *Turk. J. Chem.*, 28 (2004) 425.
21. T.P. Hoar, D.C. Mears, G.P. Rothwell, *Corros. Sci.*, 5 (1965) 279.
22. M. Schneider, S. Schroth, S. Richter, S. Höhn, N. Schubert, A. Michaelis, *Electrochim. Acta.*, 56 (2011) 7628.
23. H. Deng, R. Huang, K. Liu, X.Q. Zhang, *Electrochem. Commun.*, 82 (2017) 80.
24. A.J. Bard, L.R. Faulkner, Electrochemical methods fundamentals and applications, John Wiley, (2001) New York, U.S.A.
25. F. Aloui, F. Rehimi, E. Dumont, J. Legrand, *Int. J. Electrochem. Sci.*, 3 (2008) 676.

26. H. Matsushima, Y. Fukunaka, S. Kikuchi, A. Ispas, A. Bund, *Int. J. Electrochem. Sci.*, 7 (2012) 9345.
27. D. Zhu, C. Liu, Z.Y. Xu, J. Liu, *Chinese. J. Aeronaut.*, 29 (2016) 1111.
28. J.C. Zhang, D. Zhu, Z.Y. Xu, K.L. Zhang, J. Liu, N.S. Qu, D. Zhu, *J. Mater. Process. Tech.*, 231 (2016) 301.
29. D. Deconinck, S.V. Damme, J. Deconinck, *Electrochim. Acta*, 60 (2012) 321.
30. Y.L. Chen, X.C. Zhou, P.X. Chen, Z.Q. Wang, *Chinese. J. Aeronaut.*, 33 (2020) 1057.